

Numerical studies of International Linear Collider positron target and optical matching device field effects on beam

Sergey Antipov^{a)} and Linda Spentzouris
Illinois Institute of Technology, Chicago, Illinois 60616

Wanming Liu and Wei Gai
Argonne Wakefield Accelerator Facility, Argonne National Laboratory, Illinois 60439

(Received 19 February 2007; accepted 24 May 2007; published online 13 July 2007)

For an International Linear Collider (ILC) undulator-based positron source target configuration, a strong optical matching device (OMD) field is needed inside the target to increase the positron yield (by more than 40%) [Y. K. Batygin, Proceedings of the 2005 ALCPG and ILC Workshops, Snowmass, CO, 14–27 August 2005 (unpublished)] It is also required that the positron target be constantly rotated to reduce thermal and radiation damages. Eddy currents, produced by an OMD field in turn, interact with the magnetic field and produce a drag (stopping) force. This force not only produces heat in the disk but also creates a dipole deflecting field, which affects the beam. Therefore it is important to simulate such a system in detail to design the motor and cooling system and also a correction magnet system. In order to guide the ILC target design, an exact simulation of the spinning disk in a magnetic field is required. In this paper we present a simulation method implemented using COMSOL and compare it with the experimental results recently obtained at Stanford Linear Accelerator Center and Lawrence Livermore National Laboratory. Good agreement between the simulation and the experiment gives confidence in the validity of the method. We give detailed results on the proposed ILC target system, such as parametric studies for reduction of the power required to keep the target spinning. We present simulation results of the induced deflection field and of the reduction of the OMD field effect. © 2007 American Institute of Physics. [DOI: 10.1063/1.2752602]

I. INTRODUCTION

A spinning metal disk in magnetic field was discussed in regards to the idea of a magnetic brake. A simple empirical scaling model was developed,^{2,3} and later refined by Kachroo and Qian.⁴ However, these models only fit the low velocity region and produce large errors in the region of high rotational speed.

In this paper, we aim to solve for eddy currents induced in a conducting disk (target) spinning in the presence of external magnetic field (OMD). So far, the OMDs under consideration (either superconducting or normal) have constant magnetic fields. Our focus will be on studies and simulations of a conducting disk rotating in a constant magnetic field. This problem does not have an exact solution.

It is a challenge to simulate a spinning disk in arbitrary magnetic field. There are several possible methods to do so:

- (1) We can solve Maxwell's equations on a moving grid. However, it is very hard to implement a moving mesh in a simulation, and it can lead to numerical instabilities. To solve a stationary problem, one will have to have a mesh, uniform under rotation transformation, which will result in high memory requirements.
- (2) Another possibility is to solve the problem in a rotating frame rather than in the laboratory frame. Then the challenge is handling the magnetic field distribution, which rotates in the simulation. It can be implemented only in

a time-domain simulation. This approach requires a large mesh as well, making the simulation practically impossible to be done on a personal computer (PC).

- (3) It seems that the best way to simulate this problem is to directly include the fact that the target rotates in Maxwell's equations and solve the modified equations. However, this brings us to a nonstandard equation. Usually, for such cases, one needs to develop a custom solver. Some commercial simulation software packages allow the input of custom differential systems for a specified geometry. We used the COMSOL [finite element method (FEMLAB)] software to simulate this problem.⁵ The finite element method allows effective mesh configurations. In our case, the eddy currents are excited in the proximity of the applied magnetic field. Therefore, we use a dense mesh in the area of interest, and a less dense mesh in the remaining subdomains.

A disk rotating in a magnetic field produces an additional emf via the Lorentz force. Therefore Ohm's law has to be transformed (Lorentz transformation) accordingly:

$$\mathbf{E} + \mathbf{v} \times (\mathbf{B} + \mathbf{B}_0) = \frac{\mathbf{j}}{\sigma}.$$

Here B is the magnetic field produced by eddy currents, $\nabla \times \mathbf{B} = \mu \mathbf{j}$; B_0 is the external magnetic field, σ is the disk conductivity, and $\mathbf{v} = \omega \times \{-y, x, 0\}$ is a velocity vector field at the point (x, y, z) on the disk. Here we consider the disk spinning in the XY plane. Without static charges and disper-

^{a)}Electronic mail: antipov@anl.gov

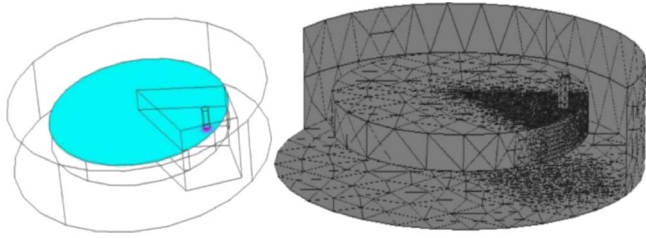


FIG. 1. (Color online) Left: exact geometry of the SLAC/LLNL experiment. Color: Magnetic field, perpendicular to the disk. Right: mesh of the simulation. Artificial region with fine mesh near the magnet.

sive dielectrics, the E field is divergence-free ($\nabla \cdot \mathbf{E} = 0$). That brings us to the equation for the induced field B :

$$\nabla^2 \mathbf{B} + \sigma \cdot \mu \cdot \nabla \times [\mathbf{v} \times (\mathbf{B} + \mathbf{B}_0)] = 0 \quad \text{or} \quad \nabla^2 \mathbf{B} + \sigma \cdot \mu \cdot \{[(\mathbf{B} + \mathbf{B}_0) \nabla] \mathbf{v} - (\mathbf{v} \nabla)(\mathbf{B} + \mathbf{B}_0)\} = 0.$$

The z component of the magnetic field decouples. This provides the grounds for approximate models for cases when x and y of induced and external fields can be neglected. We proceed to the full three-dimensional (3D) simulation of this system of three coupled differential equations.

II. SIMULATION OF SLAC/LLNL EXPERIMENT

A group of LLNL/SLAC scientists⁶ conducted a series of experiments with copper and aluminum disks with diameters of 9 and 10 in., and thicknesses of 0.9 and 1 in., respectively. The disk was rotated in the magnetic field produced by a single pole magnet of 1 cm aperture. The distance between the magnet and the disk was 0.1, 0.05, or 0.01 in. The force acting on the magnet from the spinning disk was measured using strain gauges. This force is equal to the drag force. During the experiment, the roll-off of the force at higher frequencies of target rotation that was expected from the approximate models was not observed.

We performed an exact simulation based on the method described in the Introduction. Typically this simulation consisted of two steps. First, an exact simulation of the magnet system was performed. This provided a true curl-free external magnetic field that was the same as in the experimental

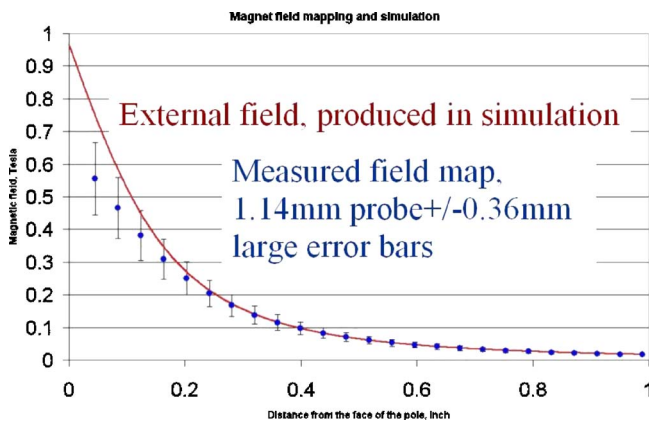


FIG. 2. (Color online) Comparison between field mapping in the experiment and simulation. Simulated field has 2000 data points per inch.

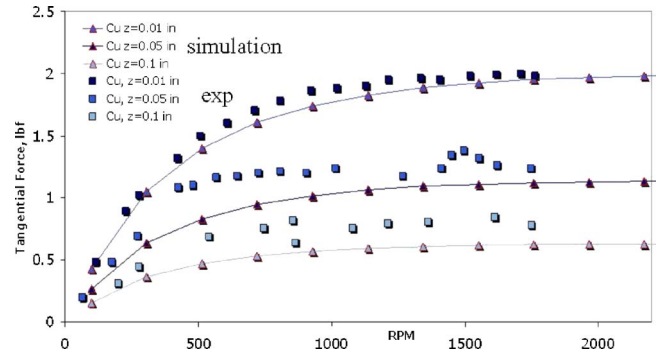


FIG. 3. (Color online) Comparison between the SLAC/LLNL experiment and 3D simulation.

setup. Then the following system of equations was solved for each needed value of angular frequency ω to obtain the induced magnetic field B :

$$\begin{aligned} -\nabla^2 B_x + \sigma \mu \omega \left[-y \frac{\partial(B_x + B_{0x})}{\partial x} + x \frac{\partial(B_x + B_{0x})}{\partial y} + (B_y + B_{0y}) \right] &= 0, \\ -\nabla^2 B_y + \sigma \mu \omega \left[-y \frac{\partial(B_y + B_{0y})}{\partial x} + x \frac{\partial(B_y + B_{0y})}{\partial y} - (B_x + B_{0x}) \right] &= 0, \\ -\nabla^2 B_z + \sigma \mu \omega \left[-y \frac{\partial(B_z + B_{0z})}{\partial x} + x \frac{\partial(B_z + B_{0z})}{\partial y} \right] &= 0. \end{aligned}$$

Postprocessing included calculation of eddy currents, force field, and integration over the disk volume to obtain the net force as a function of angular frequency of the disk.

To reduce memory requirements, an artificial subdomain was created in the simulation. The mesh is very fine in this subdomain and less fine for the rest of the geometry (Fig. 1). First a magnet system is simulated. There is a discrepancy between the simulation and the measurement near the face of the magnet. This is expected because it is impossible to measure the field near the face due to the probe size (1.4 mm) (Fig. 2). The thickness of the disk is 0.9 in.. The field inside

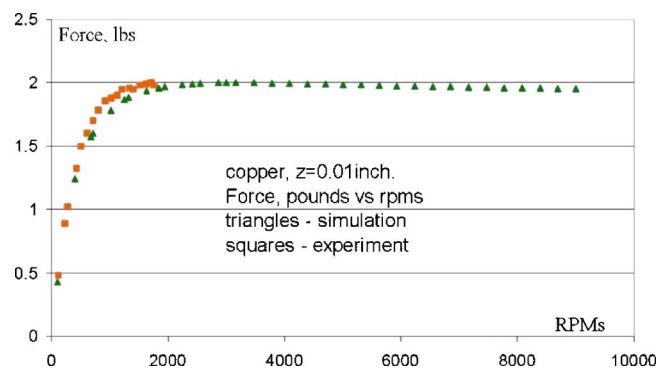


FIG. 4. (Color online) High frequency studies of stopping force behavior with SLAC/LLNL experiment geometry.

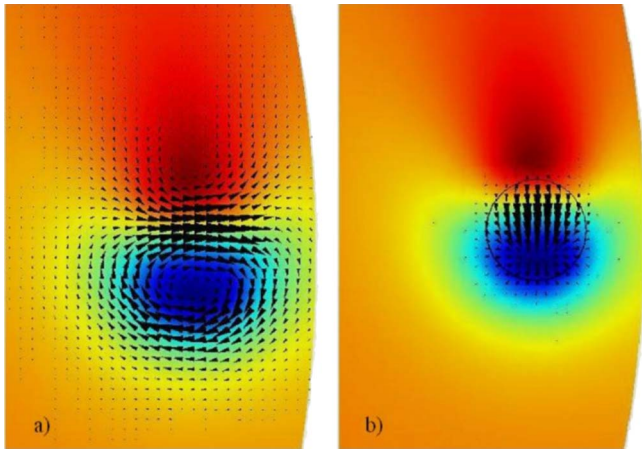


FIG. 5. (Color online) Slice in xy plane (parallel to the disk). (a) Color: induced magnetic field (z component); arrows: eddy currents. (b) Color: induced magnetic field (z component); arrows: force field; and circle: magnet pole contour.

the disk is in very good agreement with the simulated one.

The exact simulation is in very good agreement with the experimental data (Fig. 3). It shows that the roll-off is almost flat; the force does not drop much at higher frequencies. In the experiment the generator was not able to reach angular frequencies higher than 2200 rpm. The simulation not only agrees with the experiment but also predicts the drag force behavior at much higher frequencies (Fig. 4). The main component of induced magnetic field (z) has a dipole-looking configuration for low frequencies. This result and the eddy current distribution and the $j \times B_0$ [(rot B/μ) $\times B_0$] force field are presented in Fig. 5. The picture shows only the part of the disk under the magnet.

LLNL has also performed transient simulations of the *experiment.⁷ A commercial, finite element, quasimagneto-static code (Maxwell 3D Transient) with the rotational option was used. Due to the magnetostatic treatment, this code is inaccurate at high frequencies. Calculations at relatively low mesh resolution gave poor agreement with experimental force measurements. After some mesh refinement, decent agreement with transverse force experimental data was obtained for the 0.1-in.-gap spacing up to about 1000 rpm.⁸ At higher angular frequencies, a marked rollover in the drag

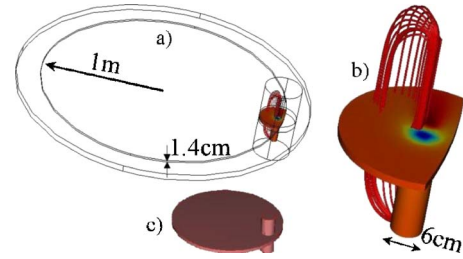


FIG. 6. (Color online) (a) ILC target exact geometry simulation. (b) Region of interest, near the solenoid. Upper half of the solenoid is not pictured to show induced field on the target (color). Streamlines: solenoidal magnetic field. (c) Complete computational domain.

force was observed. Further mesh refinement may be expected to give better agreement with the experimental results, especially at the two closer spacings.

III. SIMULATION OF THE INTERNATIONAL LINEAR COLLIDER TARGET

The International Linear Collider (ILC) positron target is a 2 m diameter, 1.4 cm thick conducting disk (Fig. 6). It rotates in the OMD magnetic field. The magnetic field reaches the value of 5 T inside the disk. We use our method to simulate this geometry.

A simulation of the solenoid has high mesh requirements. To confirm this simulation, we also simulate an ILC geometry in a strong magnetic field, produced by a magnet. The solenoid concentrates the field, and the field outside the solenoid decreases quickly. That is why we expect the field effects to be slightly higher in the case of two magnets than in the case of two solenoids.

There is a strong dependence of the drag force on the electrical conductivity of the target material. A parametric study for σ varying between copper (5.997×10^7) and titanium ($\sim 1.86 \times 10^6$) was performed. The results (Figs. 7 and 8) show that the higher the conductivity, the lower the roll-off frequency for the drag force on the spinning disk.

We calculated the power needed to keep the disk spinning at a certain frequency. It is simply the product of the drag force and linear velocity at the magnet or solenoid location. Despite the roll-off of the stopping force with frequency, the power is dominated by the ω multiplier. The force simply does not decrease fast enough.

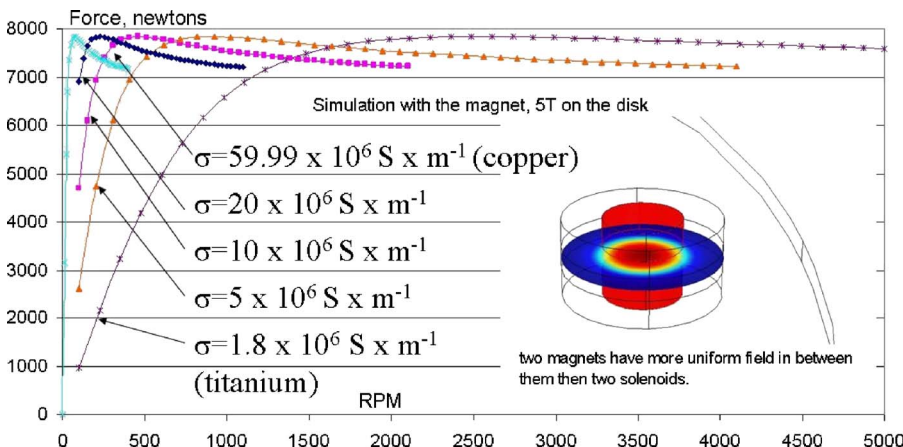


FIG. 7. (Color online) Braking force as a function of rotational frequency for various electrical conductivities. 5 T magnetic field is produced by two magnets.

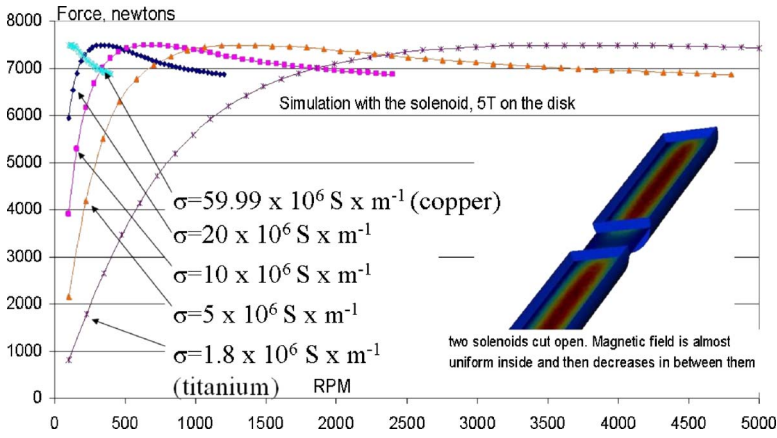


FIG. 8. (Color online) Braking force as a function of rotational frequency for various electrical conductivities. 5 T magnetic field is produced by two solenoids.

The ILC target is intended to operate at frequencies near 1000 rpm.⁹ Our results show (Fig. 9) that it requires about 800 kW to keep the solid target spinning at this frequency. This number has to be brought down for the design to be more realistic. This can be achieved by substituting the disk with a ring. This reduces the effective area where the eddy currents can be excited and brings down the power required to keep the target rotating.

Parametric studies of the ring configuration were also performed. We varied the conductivity, σ (1.5×10^6 and 3×10^6), the target (ring) width (1.5 and 3 cm), and the magnet aperture (3, 6, and 12 cm). The results show encouraging numbers (Table I). As expected, a low σ and a small target area require much less power to keep the target rotating. The frequency dependence of the drag force is shown in Fig. 10.

Another important effect associated with the target rotation is the attenuation of the total field inside the target. The field from the OMD, B_0 , induces the eddy currents. The eddy currents, in turn, produce the field B . According to Lenz's law, this field tries to reduce the external field. This effect depends strongly on the rotational frequency. Figure 11 shows the major component (z) of the total field ($B+B_0$) as a function of z at different rotational frequencies for a 3 cm wide target with a 3 cm aperture magnet with external field of 5 T. The faster the target rotates, the lower the field. Nevertheless, at 980 rpm, which is in the range of planned operating frequencies, the total field is 2 T. This is still acceptable for positron yield.¹

At this point, the transverse components of the induced

field become the main issue for target development. They create the deflection field. Figure 12 presents x and y components of the induced magnetic field 5 mm away from the surface of the target. This is a first order magnitude effect (~ 0.2 T). As can be seen in Fig. 12, it is B_y field that will deflect the beam. Particles with low energies will be steered more dramatically. The lowest captured energy of the positron from the target is 3 MeV. Further, we simply integrate the equation of motion with the Lorentz force, produced by a B_y component of magnetic field along the particle path. The maximum deflection, neglecting the focusing properties of the solenoid in this case, is 3 mm on the length where B_y is still significant. A correction system can be designed based on the simulation results to steer the beam back. Since the deflection is dominated by a single component of magnetic field, a simple dipole magnet can do the job.

IV. DRAG FORCE RISE EFFECT IN ULTRAHIGH FREQUENCY REGION

Exact simulations of the spinning disk in a magnetic field revealed an interesting effect that, to our knowledge, has not been reported. Previous work on magnet braking based on approximate models defined two regions of asymptotic behavior. A low frequency region is characterized by a drag force rising with increasing frequency, and a high frequency region has the drag force decreasing with increasing frequency. Then an approximate equation for the critical frequency between low and high frequency regions was presented.

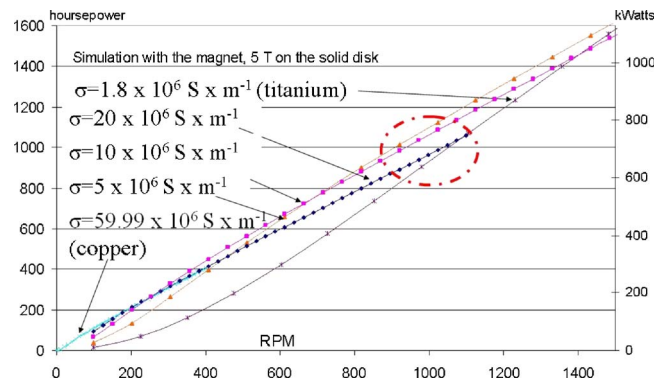


FIG. 9. (Color online) Power required to keep the target spinning in 5 T magnetic field.

TABLE I. Results for parametric studies of various target widths, magnet apertures, and conductivities.

	Ring width: 1.5 cm	Ring width: 3 cm
$\sigma = 3 \times 10^6$, 5 T field		
Magnet aperture: 3 cm	278 kW at 980 rpm	488 kW at 980 rpm
Magnet aperture: 6 cm	300 kW at 980 rpm	657 kW at 980 rpm
Magnet aperture: 12 cm	325 kW at 980 rpm	770 kW at 980 rpm
$\sigma = 1.5 \times 10^6$, 5 T field		
Magnet aperture: 3 cm	170 kW at 910 rpm	332 kW at 910 rpm
Magnet aperture: 6 cm	172 kW at 910 rpm	433 kW at 910 rpm
Magnet aperture: 12 cm	175 kW at 910 rpm	463 kW at 910 rpm

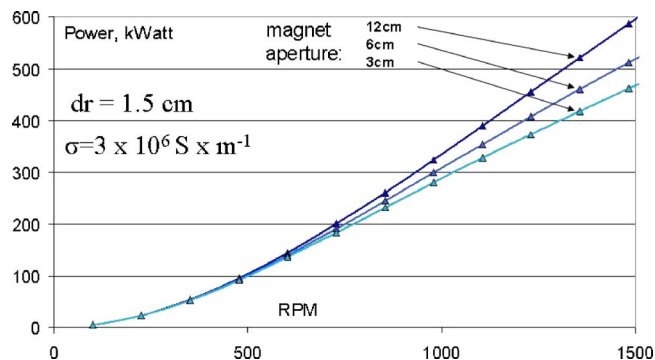


FIG. 10. (Color online) Required power for $\sigma=3 \times 10^6$, 3 cm width of the target, and 5 T magnetic field, with 3, 6, and 12 cm aperture of the magnet.

Our exact simulations also show the rise of the drag force in the low frequency region and the roll-off in the high frequency region. However, the region for even higher frequency (ultrahigh frequency region) of the rotation was not previously studied. We show that, at some point, the drag force starts rising again. Figure 13 shows the results from a simulation of ILC positron target geometry, made of copper in 5 T external magnetic field. We also plot a z component of total field (external+induced) at various frequencies to explain the effect.

At low frequency (point *a* in Fig. 13), the eddy currents are tiny, they produce a very small field, and therefore the total field almost equals the external field of the magnet. We see that it is concentrated under the magnet. Once the frequency goes higher (point *b*), the induced field starts to cancel the external field partially and extends from underneath the magnet as the disk rotates. The roll-off happens when the frequency is high enough, so the induced field cancels out the external field and lies mostly outside the magnet. The spinning disk drags the field out from underneath the disk, so to speak. The ultrahigh region (point *d*) brings another effect into play. The field, which got dragged out from underneath the disk, makes a full rotation and finds itself under the mag-

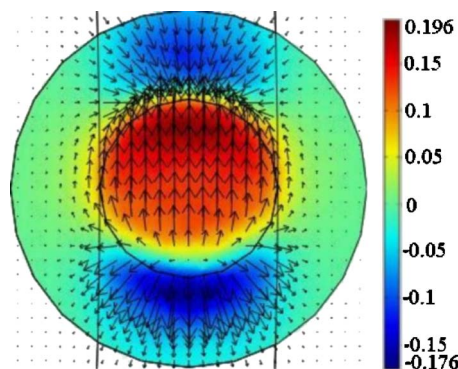


FIG. 12. (Color online) Transverse components of induced field (T) (Color: B_y ; arrows: $\{B_x, B_y\}$), plotted at 5 mm from the surface of the target at 980 rpm frequency. Inner ring is the projection of the magnet.

net again. This portion contributes to the drag force ($j \times B_0$ or $[(\text{rot } B/\mu) \times B_0]$). This explains why the force starts rising again.

Studies at even higher frequencies, than the ones we investigated, require large amounts of memory because of the mesh requirements. The frequency term is a multiplier in the system of equations we used for the simulation. Therefore once it becomes larger than some critical value, the Laplacian term in the equations becomes much smaller than other terms. At this point, the mesh has to be improved; otherwise, the simulation does not converge.

However, we can expect that there will be another roll-off at higher frequencies, followed by a new rise. This will go on with decreasing amplitudes of oscillations until the initial magnetic field is smeared uniformly and a constant force is achieved.

V. SUMMARY

We have developed a model that numerically solves the problem of a conducting disk spinning in a magnetic field. The simulation was checked against the SLAC/LLNL experi-

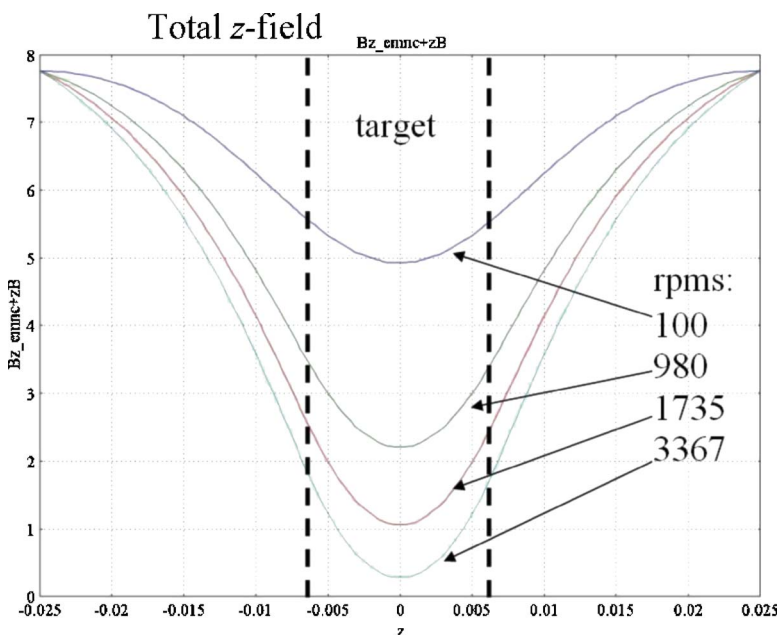


FIG. 11. (Color online) Total magnetic field (T) (z component) across the target (m) at 100, 980 (ILC design), 1735 (critical), and 3367 rpm.

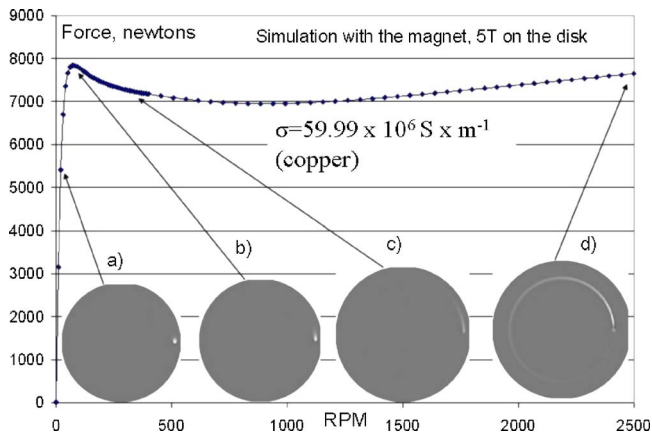


FIG. 13. (Color online) Rise of the drag force in ultrahigh speed region. Force (N) as a function of rotational frequency. Grayscale plots: total field at various frequencies. (a) Rotation is slow; total field is practically equal to external field. Once the speed of rotation increases [(b) and (c)], it cancels out the external field under the magnet. The field is dragged out from under the magnet. At ultrahigh frequencies (d), the total field makes a full turn and contributes to the total drag force again, causing the rise of a drag force.

ment. Very good agreement is reported. We have performed general studies for the ILC positron target. Parametric studies were done. These simulations help to determine a realistic design for the ILC positron target: OMD aperture, thickness of the rim in a ring configuration of the target, and conductivity of the target.

We discussed several effects associated with the target rotation and their effect on the beam. Reduction of OMD

field by the induced field can be made less dramatic at lower rotational frequencies. The deflection field induced by rotation can be simulated. Based on the simulation, a correction system can be developed.

An interesting effect at ultrahigh frequencies of the disk rotation was illustrated and explained.

ACKNOWLEDGMENTS

We are very grateful to John Sheppard and Vinod Bharadwaj of SLAC for bringing the problem to our attention and for helpful discussions. We would also like to thank Jeff Gronberg, Tom Piggot, David Mayhall, and Jianguo Ma for the exciting discussions. This work is partially supported by the U.S. DOE, Division of High Energy Physics, under Contract No. DE-AC02-06CH11357, and the National Science Foundation, Grant No. 0237162.

¹Y. K. Batygin, Proceedings of the 2005 ALCPG and ILC Workshops, Snowmass, CO, 14–27 August 2005 (unpublished).

²J. H. Wouterse, *IEEE Proceedings B: Electrical Power Applications*, July 1991 (IEEE, New York, 1991), Vol. 138, pp. 153–158.

³W. R. Smythe, Transactions of AIEE (unpublished), Vol. 61, pp. 681–684.

⁴P. Kachroo and M. Qian, *IEEE Conference on Intelligent Transportation Systems, ITSC'97* (IEEE, New York, 1997), pp. 391–396.

⁵COMSOL Multiphysics user guide (www.comsol.com).

⁶W. T. Piggott, S. Walston, and D. Mayhall, LLNL Report No. UCRL-TR-224467, 2006 (unpublished).

⁷D. J. Mayhall, W. Stein, and J. B. Gronberg, LLNL Report No. UCRL-TR-221440, 2006 (unpublished).

⁸D. Mayhall, (private communication).

⁹Summary of work group 3a, Proceedings of 2005 ALCPG and ILC Workshops, Snowmass, CO, 14–27 August 2005 (unpublished).